ELSEVIER

Physica C 265 (1996) 341–352

PHYSICA C

Manufacturing and microstructural aspects of CO_2-laser processed $YBa_2Cu_3O_{7-\delta}$ superconductors

D.I. Pantelis *, G. Pantazopoulos

Manufacturing Technology Division, Department of Mechanical Engineering, National Technical University of Athens, Athens, Greece

Received 21 March 1996

Abstract

A 3.2 kW continuous-wave CO_2 laser was employed in order to achieve the surface modification of $YBa_2Cu_3O_{7-\delta}$ superconducting pellets as well as for the fabrication of thick superconducting coatings (paths) in the Y-Ba-Cu-O system on silver substrate, with prospect application into the construction of electrical and/or electronic circuits. The laser manufacturing technique is reported and discussed in terms of irradiation-material interactions and process optimization. Subsequently, the resultant macro- and microstructure, including phase transformations, morphological aspects, interface phenomena and defect-structure were investigated and correlated with the various laser processing parameters. Preliminary resistivity measurements were conducted in order to evaluate the superconductivity of the irradiated ceramic materials after appropriate heat treatment in oxygen atmosphere.

1. Introduction

Since the discovery of high-T_c superconductors (HTS) in the Y-Ba-Cu-O system [1], numerous efforts have been made to synthesize new superconductors with higher transition temperature and on the other hand to develop novel processing routes for the manufacturing of bulk ceramic superconducting materials. However, developments of superconducting material fabrication considering the solid-state reaction techniques lead to polycrystalline (granular) superconductors possessing many serious defects, i.e. porosity, microcracking, normal/insulating phases concentrated at the grain boundaries, etc., resulting, therefore, in the interruption of the supercurrent flow and in the degradation of the critical current density (J_c).

Thick- and thin-film processing techniques are dedicated to develop superconducting coatings of various types and thicknesses with improved microstructure and therefore better transport properties. Several production methods have been proposed and demonstrated, e.g. molten-oxide processing [2], rapid-quench method [3], tape casting [4], spray pyrolysis [5], screen printing [6], plasma-spraying [7], co-evaporation [8], RF-sputtering [9], chemical-vapour-deposition [10] and laser processing [11–23].

Various types of laser have been used for the synthesis and also for the fabrication of HTS coatings in both Y-Ba-Cu-O and Bi-Sr-Ca-Cu-O systems. The laser-ablation technique has been proposed for the development of highly stoichiometric HTS thin-film on various substrates, by means of the excimer laser-material photochemical interactions

* Corresponding author. Fax: +30 1 381 3897.

PII S0921-4534(96)00335-8

[11–17]. The Nd^{3+}-YAG laser was employed to stimulate the growth kinetics of the (2223)-phase in Bi-Sr-Ca-Cu-O system [18,19]. CO_2 high power laser, working in a continuous-wave mode, has been used to a lesser extend in the field of HTS processing as compared to the other types of lasers, according to the literature [20–23], although many industrial applications are conducted using this type of laser, mainly machining, welding and hardfacing [24]. CO_2-laser irradiation, emitting in the IR spectrum ($\lambda = 10.6$ μm), leads to thermal effects interacting with the condensed matter. First, surface melting occurs followed by rapid resolidification eliminating, not only, the various defects originated from the granularity of the HTS materials, but also resulting in the formation of a fine-grained microstructure having also an advantageous crystallographic orientation [20–22].

To improve the current density in superconductors an increase in pinning force is necessary. Based on previous knowledge, the supercurrent flow is limited near the surface of the superconducting materials. Therefore, the CO_2-laser surface treatment of a superconductor is adopted by the authors that improves the surface and near-subsurface physical properties, which may lead to the increase of transport properties.

In this paper, presented are the manufacturing and the microstructural aspects of a CO_2 laser irradiated $YBa_2Cu_3O_{7-\delta}$ pellet and the possibility of the application of CO_2 laser processing to produce thick superconducting coatings which is discussed in terms of process optimization and microstructure evolution. Preliminary electrical measurements, after suitable post heat treatment, have indicated possible applications of these components into the construction of electrical and/or electronic circuits.

2. Experimental

2.1. Materials

(i) *HTS pellet.* Superconducting powder corresponding to $YBa_2Cu_3O_{6,8}$ compound was prepared according to the well-known solid-state reaction technique, starting from stoichiometric quantities of $BaCO_3$, Y_2O_3 and CuO. After the synthesis, the resultant powder was reground in an agate mortar and sintered at 875°C for 2 h and then cooled down with a 10°C/h cooling rate. Cold pressing was followed using a hydraulic press to form disk-shaped ceramics (pellets) of a 25 mm diameter and 2.5 mm thickness. Electrical characterization of the bulk ceramic was conducted in a liquid Helium cryostat indicating sharp resistive transition at 90 K. The exact oxygen deficiency ($\delta = 0, 2$) was derived from suitable thermogravimetric analysis (TGA).

(ii) *HTS coatings.* In order to develop thick HTS coatings, silver plates of dimensions $50 \times 12 \times 3$ mm^3, were used as substrates. The ceramic powder produced after appropriate grinding was predeposited onto a grooved silver plate without any surface preparation. Subsequently, the powder was slightly pressed with a pestle in order to achieve the maximum bulk density before the laser treatment.

2.2. Laser processing

The laser used was a high power c.w. CO_2 laser, with a maximum output power of 3.2 kW. The

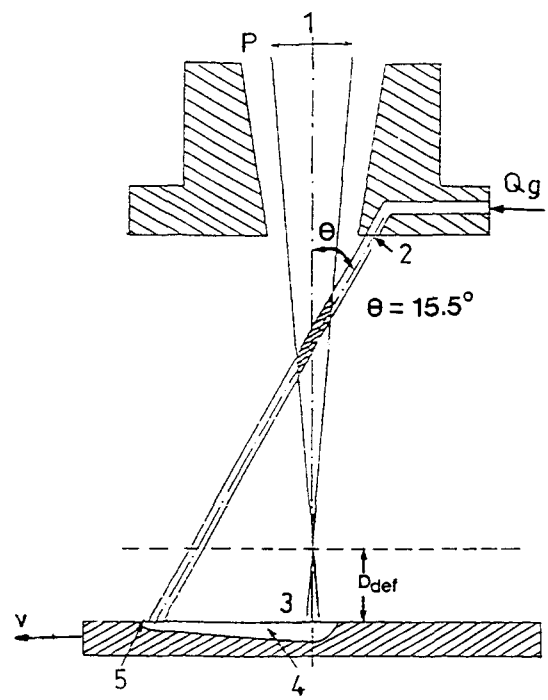

Fig. 1. Schematic illustration of the laser experimental set-up; 1: laser beam characteristics, 2: inert gas flow-rate, 3: laser-matter interaction, 4: cooling of the molten pool, 5: solidification.

energy distribution is of TEM_{01} type and the wavelength of the emitted irradiation was 10.6 μm. The process parameters used for all the series of experiments were varied under the following domains:
laser power (P): 1–3 kW;
laser beam displacement velocity (v): 0.5–4

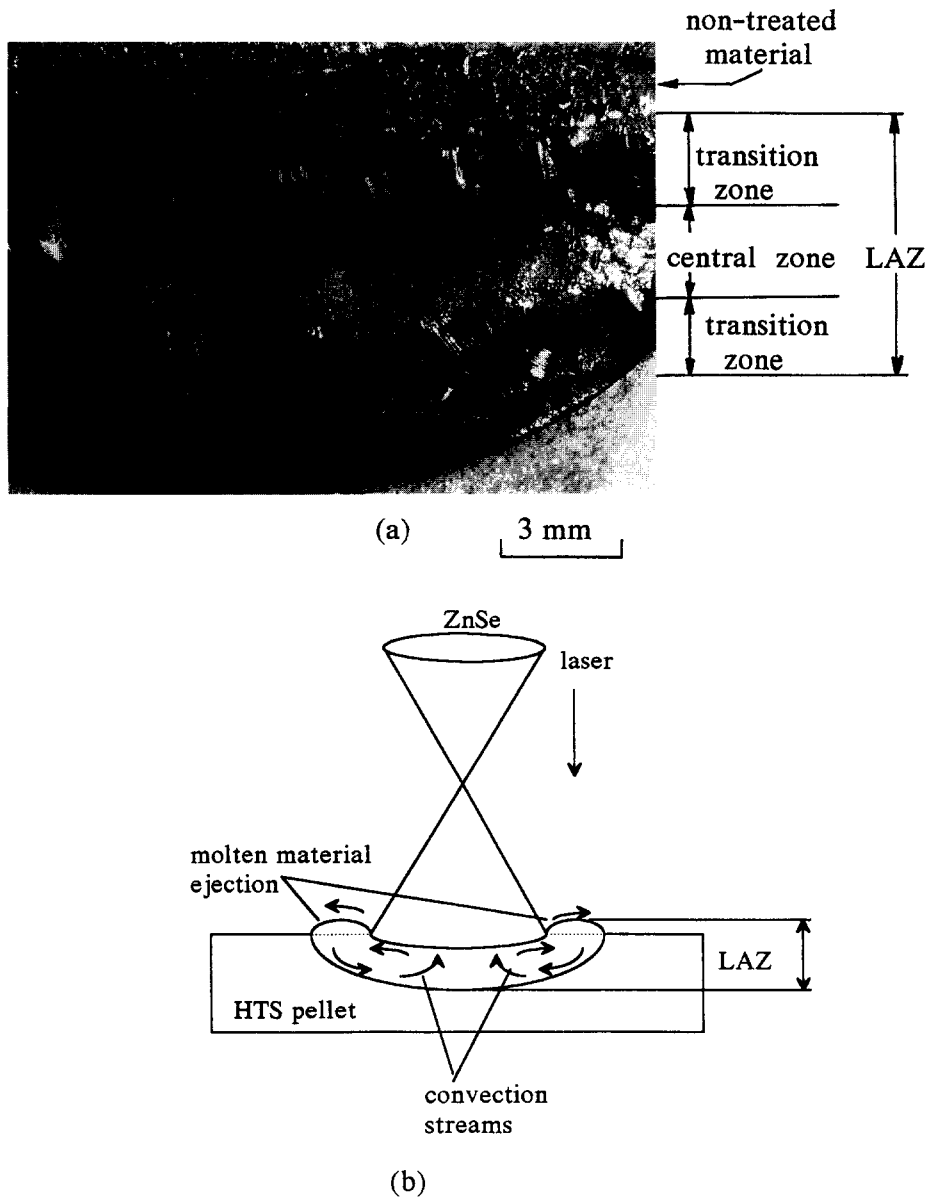

Fig. 2. (a) Optical micrograph showing a plane view of the laser treated HTS pellet under the optimum processing conditions; $P = 1$ kW, $v = 1$ m/min and $D_{def} = 30$ mm. (b) Schematic illustration of the melt-zone formation during laser irradiation (cross-section).

m min^{-1};
defocus distance (D_{def}): 17–30 mm;
laser spot diameter > 3 mm.
Argon was used as a shielding gas under a constant flowrate (Q_g) of 4 l/min.

Fig. 1 is a schematic representation of the laser experimental set-up, illustrating a general schema of the laser–matter interaction, showing also the process parameters mentioned above.

2.3. Post-processing heat treatment

Appropriate heat treatment in oxygen atmosphere was carried out under the following conditions:
heating at 907°C for 20 h;
slow cooling from 907 to 510°C with 1°C/min cooling rate;
staying at 510°C for 50 h;
slow cooling from 510°C to the room temperature with 1°C/min.

2.4. Characterization methods

The macro- and microstructures of the laser irradiated ceramics were studied by means of optical metallography and scanning electron microscopy (SEM). Energy Dispersive X-ray Analysis (EDAX) was also employed for further chemical characterization of the various microstructural features revealed by SEM. X-ray diffraction (XRD) using CuK_α monochromatic radiation was provided for the analysis and identification of the various phases and constituents induced by laser irradiation. Finally, preliminary resistivity measurements were carried out in a liquid Helium cryostat using the classical four-probe technique, with a current intensity equal to 10 mA.

3. Results and discussion

3.1. Laser irradiated $YBa_2Cu_3O_{7-\delta}$ pellet

Numerous experimental series took place in order to determine the optimum set of the laser processing parameters. The optimum laser processing parameters were, therefore, selected based on the following criteria:
(a) maximum orthorhombic phase content;
(b) minimization of cracks and porosity;
(c) optimal adhesion of the laser modified layer to the substrate;
(d) lack of specimen dimensional distortion;
(e) accentuation of the crystallographic orientation;
(f) uniform microstructure induced by laser irradiation.
According to the above criteria the optimum laser processing conditions are as follows: $P = 1$ kW, $v = 1$ m/min and $D_{def} = 30$ mm.

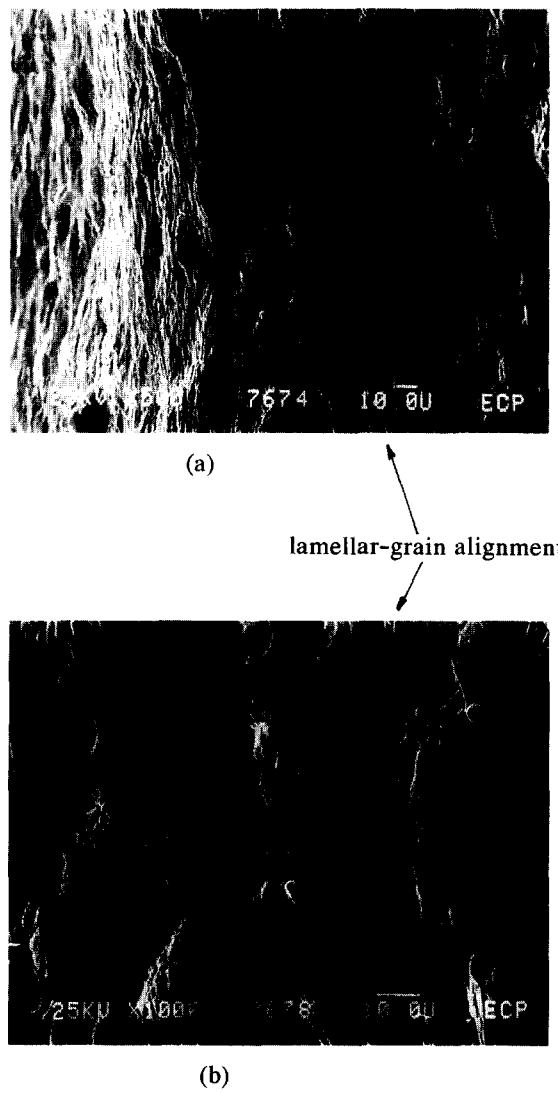

Fig. 3. (a) SEM micrograph of the laser-affected zone under the optimum processing conditions (plane-view) and (b) detail of (a).

The plane view macrostructure of the optimum laser track is presented in Fig. 2. The laser-affected-zone (LAZ), 6.4 mm wide (maximum), can be divided in to two dinstict zones:
the central zone (3.0 mm) which is nearly smooth and consists of very fine grains, and
the boundary or transition zone (3.4 mm) which is rough and consists of columnar parallel-oriented crystals.
The heterogeneity in surface topography is resulted from the non-uniform laser-beam energy spatial distribution (annular). Therefore, the higher energy concentration at the center of the laser spot leads to steeper thermal gradients and higher cooling and solidification rates. The rapidly solidified central zone is much more refined and smooth compared to the boundary zone; cracking tendency is often apparent in this zone due to the high residual tensile-stress fields induced by laser treatment (thermal and solidification stresses). Furthermore, the boundary zone morphology is similar to the so-called columnar zone found in casting processes and it is formed due to the lateral heat conduction. During laser-HTS interaction, part of the molten material is ejected, forming "lips" surrounding the central melt-zone after subsequent solidification; the rapid cooling is driven by mechanisms of conduction (heat transfer to the substrate) and convection (heat transfer occurs with relative mass transfer into the molten pool), see Fig. 2b. The resultant surface roughness is therefore increased due to the laser-induced surface topography (Fig. 2a).

Scanning electron microscopy of the surface of the LAZ revealed a wavy texture consisting of very fine lamellar crystallites, with interlamellar spacing less than 3 μm (Figs. 3a,b), while intense preferred orientation between the lamellae is present following the direction of the applied thermal gradient. The accentuated orientation helps the current conduction through the parallel-arranged *ab* crystallographic planes and, therefore, elevates the critical current density in high-T_c superconductors. Fig. 4a shows a fractured cross-section of the optimum laser track, showing the microstructure depending on the depth below the irradiated surface. The LAZ (700 μm) is morphologically uniform and consists of very fine

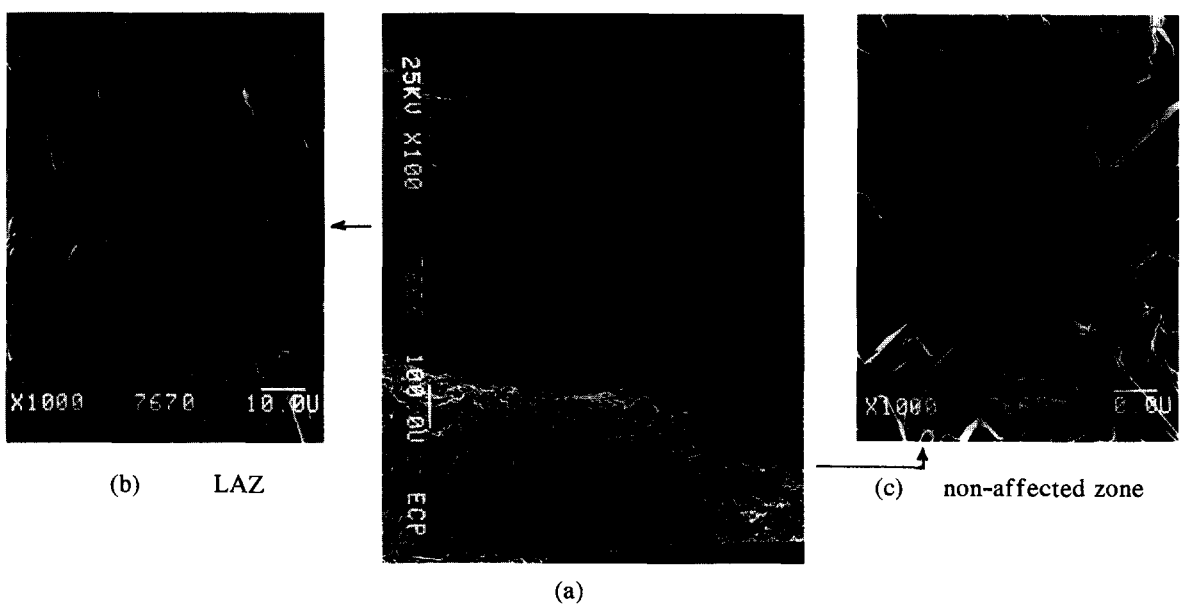

Fig. 4. SEM micrographs showing the various microstructural features revealed after the laser treatment of the HTS pellet under the optimum conditions; (a) fractured cross-section, (b) detail of the laser-affected zone and (c) detail of the non-affected zone (initial microstructure).

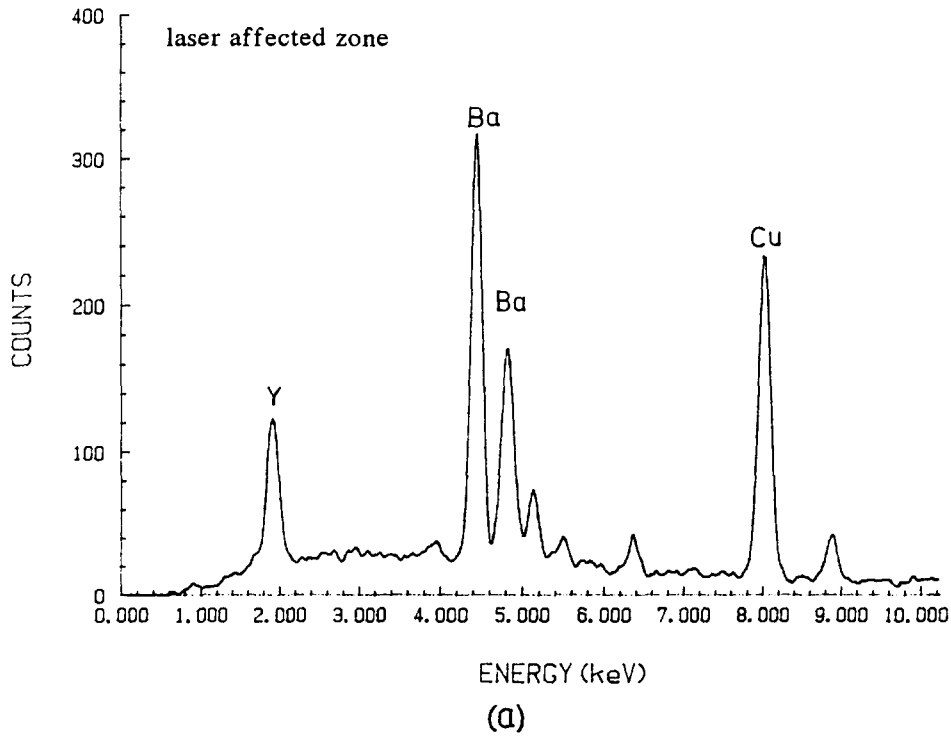

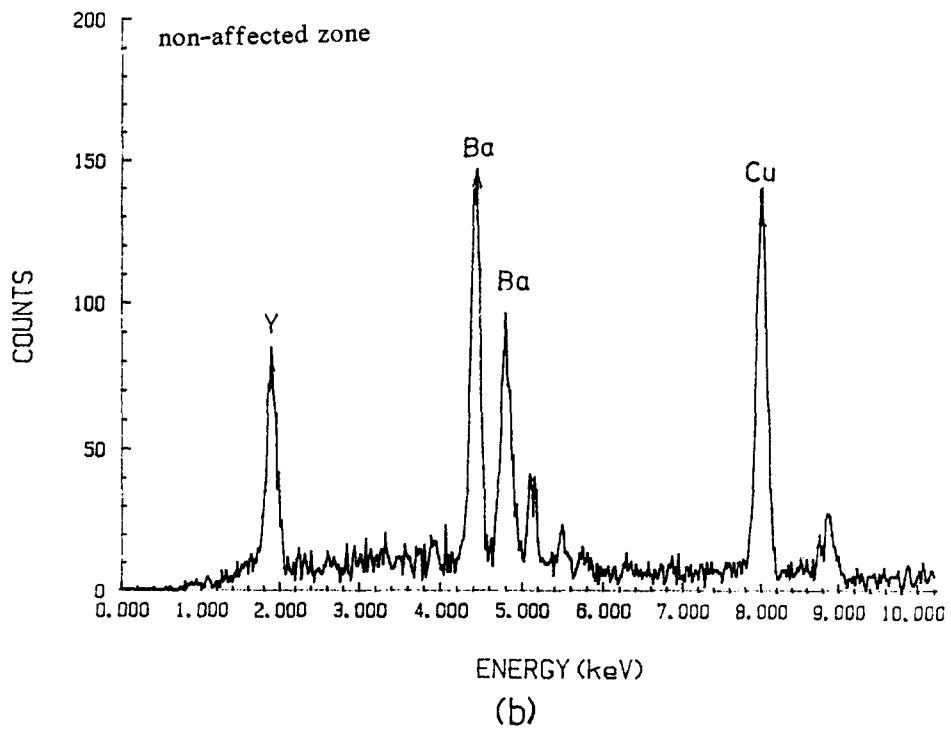

Fig. 5. (a) EDAX spectra of the laser-affected zone and (b) of the unaffected zone.

crystallites stack into each other, after laser melting and resolidification, resulting in a very high bulk density (Fig. 4b). The following zone (Fig. 4c) is the unaffected zone representing the initial sintered microstructure and comprised of weakly joined coarse prismatic crystals, with very low bulk density. The nearly tetragonal crystal morphology is very common to the perovskite minerals, such as $CaTiO_3$.

Energy dispersive X-ray analysis carried-out in the LAZ (Fig. 5a) indicates a relative increase in Ba-content with respect to the other elements (Y and Cu) compared to the non-affected zone (Fig. 5b). Such a result may be explained taking into account the possibility of the formation of Ba-rich phases, i.e. $BaCuO_2$, during 123 phase partial transformation.

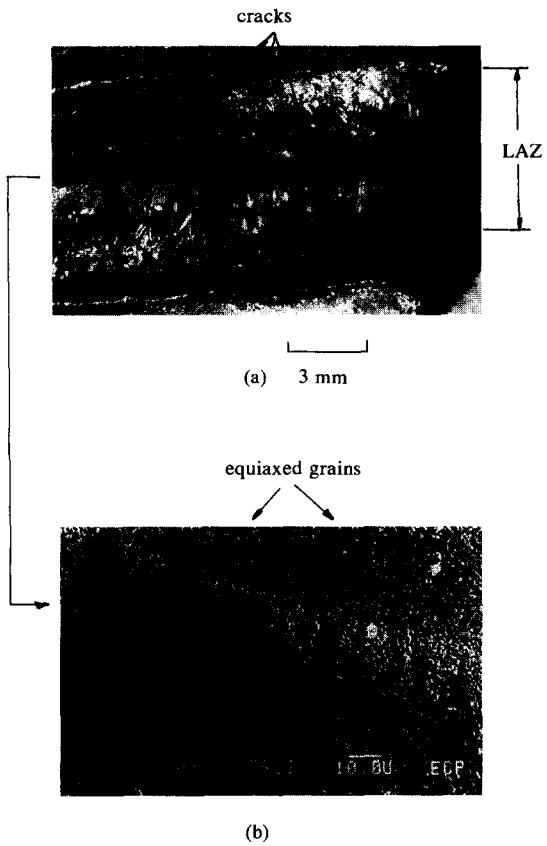

Fig. 6. (a) Optical micrograph showing a plane view of the laser treated HTS pellet under the following conditions: $P = 3$ kW, $v = 4$ m/min and $D_{def} = 30$ mm. (b) Detail of the laser-affected zone; equiaxed nanocrystalline microstructure.

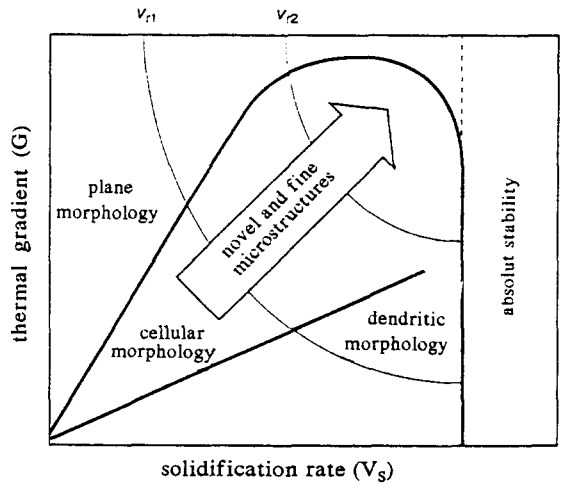

Fig. 7. Diagram representing the evolution of the microstructure as a function of thermal gradient (G) and solidification rate (V_s); V_{r1} and V_{r2} are contours of constant cooling rate.

Increasing the laser-beam displacement velocity (from 1 to 4 m/min) and the laser beam power (from 1 to 3 kW) extremely fine and dense microstructures can be developed due the rapid solidification process. The corresponding plane view of the laser track is shown in Fig. 6a; parallel-crack initiation almost perpendicular to the laser scanning speed direction is apparent in this case. The corresponding microstructure of the LAZ is extremely fine showing the presence of near-nanocrystalline equiaxed grains with diameter less than 1 μm in size (Fig. 6b). The resultant refinement of the microstructure can be

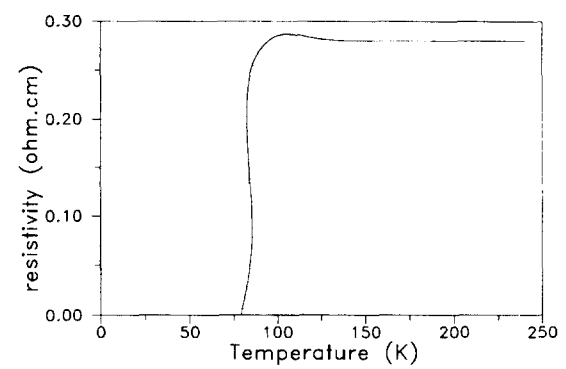

Fig. 8. Evolution of the resistivity as a function of temperature after appropriate heat treatment, for the HTS pellet.

explained taking into consideration the diagram presented in Fig. 7. It is evident that, when the laser beam power and speed are increased, the resultant thermal gradient (G) and cooling rate (V_r) are increased too, tending, therefore, to produce a very fine and/or a novel microstructure, see also Ref. [24].

Four-point resistivity measurements, performed after appropriate heat treatment, show sharp transition at an onset critical temperature of 90 K, while the corresponding transition width is relatively narrow up to 10 K (Fig. 8).

3.2. Laser manufacturing of $YBa_2Cu_3O_{7-\delta}$ coatings

The optimum laser processing conditions were also selected, after a great number of experimental series, according to the above mentioned criteria

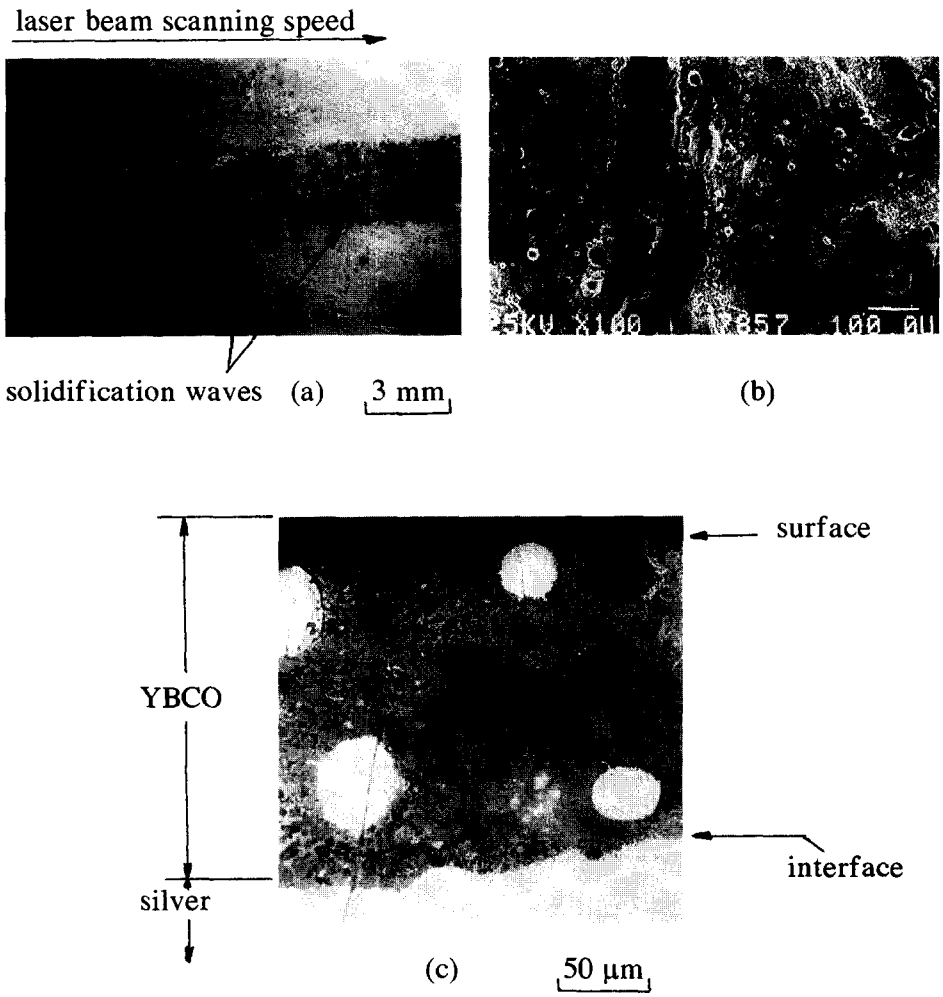

Fig. 9. (a) Optical micrograph showing a plane view of the laser fabricated HTS path under the optimum conditions: $P = 1$ kW, $v = 0.5$ m/min and $D_{def} = 17$ mm. (b) SEM micrograph presenting a detail of (a); and (c) optical micrograph showing a polished cross-section near the HTS/silver interface.

(paragraph 3.1). The corresponding optimum laser process parameters are the following ones: $P = 1$ kW, $v = 0.5$ m/min and $D_{def} = 17$ mm.

The optimum laser treatment conditions result in a continuous, dense and crack free superconducting ceramic path, 3 mm wide and having a thickness varying between 200 and 250 μm displaying also satisfactory adhesion with the substrate (Fig. 9a–c). The HTS-silver interface is free of cracks and delaminations (mainly in the centre of the track), while thermally activated silver diffusion forms metallurgical bonds with the ceramic, strengthening, therefore, the adhesion of the superconducting coating (Fig. 9c). A top-view of this HTS path is shown in Fig. 9a, indicating a characteristic solidification wave pattern, which is a very common phenomenon in laser melt-pool rheology, see also a detail in Fig. 9b. Steep thermal gradients, induced by laser beam, lead to melting and subsequent rapid resolidification of the laser melted zone. The extremely high solidification rates result also here in the creation of novel and very fine-grained microstructures. The presence of very fine dendrites, found on the surface (and reaching a depth of 100–150 μm beneath surface) of this coating (Fig. 10a), indicates the microcrystallinity resulted from the very high solidification rates. Another different type of morphology existing at a higher depth (> 150 μm), consists mainly of *radiating aggregates*, i.e. needle-like crystals grown together starting from the same nucleation point, like a fringe (Fig. 10b). The dendritic solidification occurring at the near-surface region may be triggered by the higher constitutional undercooling, i.e. lower ratio G/V_s (G: thermal gradient, V_s: solidification rate).

X-ray diffraction was carried out on the surface of the laser fabricated coatings. Fig. 11 is the X-ray diffraction pattern corresponding to the optimum HTS coating, which displays the maximum superconducting phase content. However, normal (non-superconducting) secondary phases, like 211 (Y_2BaCuO_5) and Y_2O_3 phases and silver have also been detected. The widening of the principal reflection peak of the 123 phase, at 32.7°, confirms the existence of the defect-structure: lattice defects and dislocation substructures caused by the laser irradiation and rapid thermal cycle, microstructural refinement and possible incompleteness in crystallinity and oxygen loss

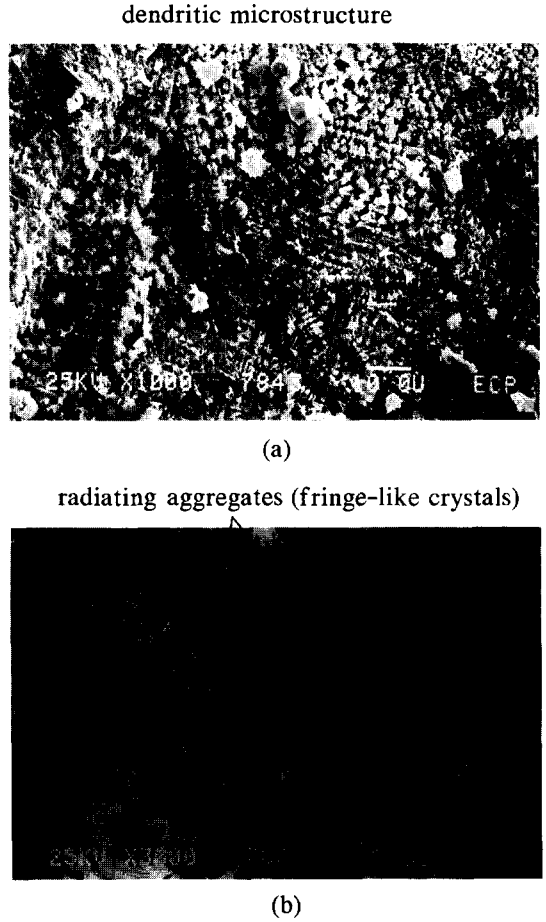

Fig. 10. SEM micrographs of the laser fabricated HTS paths, showing (a) the dendritic microstructure at the near-surface region and (b) the microstructure, consisting of radiating aggregates, at a higher depth below the laser irradiated surface.

are the main structural defects reported also in the relevant literature [22–25].

Microscopical observations, realized on various polished cross sections, of the optimum coating, reveal a complex mosaic structure resulted from laser surface modification. The most representative feature is shown in Fig. 12. This mosaic microstructure, composed of different grain morphologies and sizes, resulted from phase transformations and diffusion phenomena associated to melting and rapid solidification processes induced by laser irradiation. The coarse light grains, of 10 μm size, correspond to initial superconducting powder particles predeposited on silver substrate. The tiny gray grains, less than 1

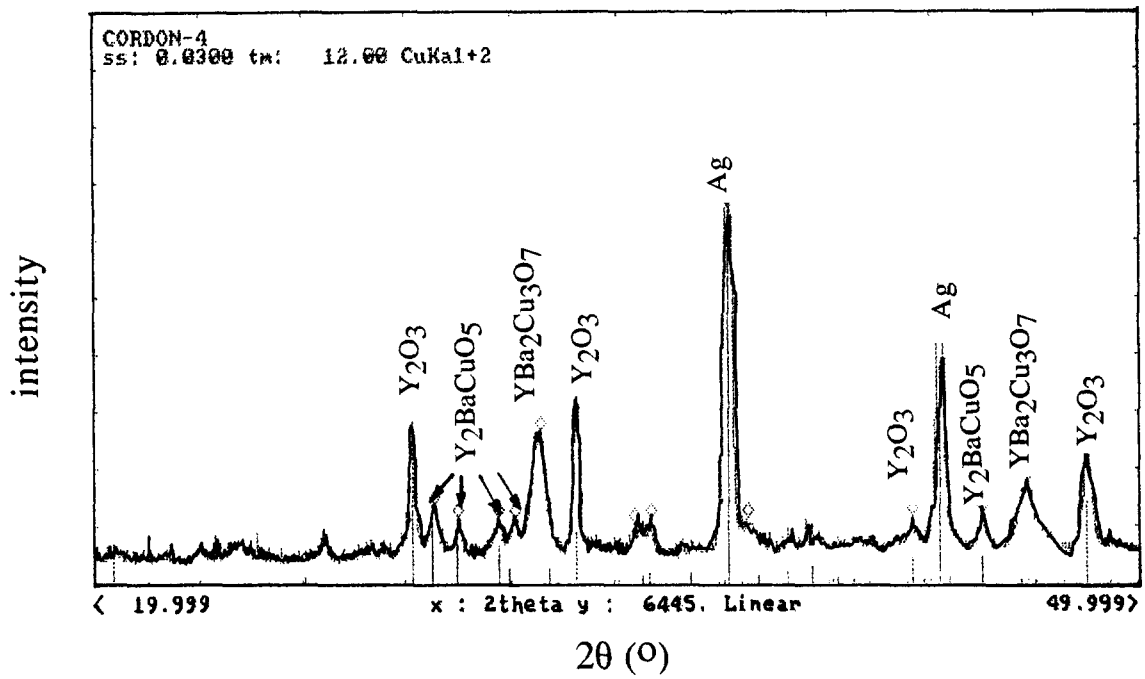

Fig. 11. XRD pattern of the optimum laser fabricated HTS path; $P = 1$ kW, $v = 0.5$ m/min and $D_{def} = 17$ mm.

μm size, which compose the greater fraction of the examined surface area, correspond to recrystallized grains resulting from rapid solidification. The observed microstructural refinement has led also to the increase of the bulk density of the superconducting coating. However, taking into consideration the XRD pattern (Fig. 11), the presence of secondary phases (Y_2O_3 and/or Y_2BaCuO_5, appearing as dark grains, due to partial 123 orthorhombic phase decomposition) is inevitable, as reported also in Ref. [23]. The formation of non-superconducting secondary phases leads, unfortunately, to the decrease of the critical

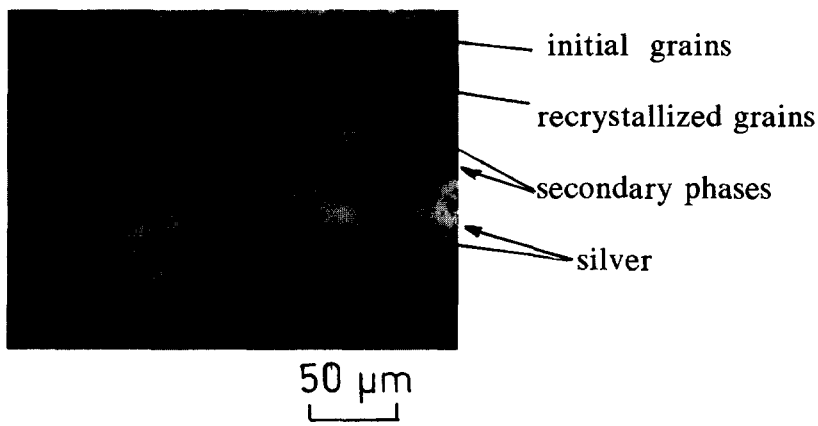

Fig. 12. Optical micrograph showing a polished cross-section of the optimum HTS path.

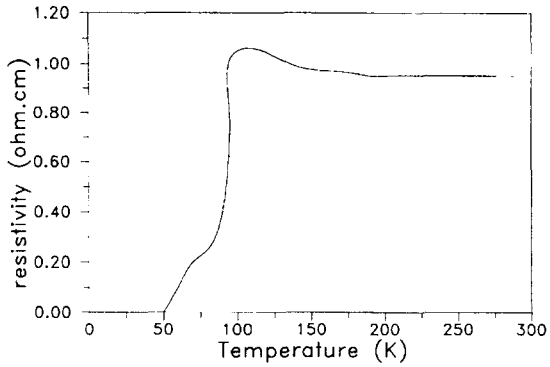

Fig. 13. Evolution of the resistivity as a function of temperature after appropriate heat treatment, for the laser fabricated HTS coating.

current density. Silver diffusion and mixing with the substrate, mainly at the liquid state, results in the formation of silver islands (white areas).

Post-processing heat treatment in oxygen atmosphere is necessary to restore the oxygen stoichiometry and improve the crystallization of the 123 orthorhombic phase. The resistivity evolution as a function of temperature, recorded after the heat treatment, and measured employing the conventional four-probe technique at liquid helium, shows a superconductive transition at an onset temperature of 90 K, while the offset critical temperature is very lower, around 50 K (Fig. 13). The observed "tailing effect", leading to $\Delta T_c = 40$ K, can be mainly attributed to the well known weak-link behaviour due to the presence of secondary phases.

4. Conclusions

An attempt was made to study the laser surface modification of a $YBa_2Cu_3O_{7-\delta}$ superconducting pellet and fabricate HTS thick-films on silver substrate for electrical and/or electronic applications by means of a 3.2 kW CO_2 laser. Summarizing the above mentioned results the following conclusions may be reached:

(1) In the case of the HTS pellet, the laser process parameters affect strongly the type and the size of the resultant morphology. Melting and subsequent rapid solidification processes create a complex microstructure and non-equilibrium constituents. Nano-crystalline grains and strongly oriented lamellar morphologies are some of the most characteristic microstructural features found in the laser-affected-zone of the superconducting pellet. Optimization of the laser process parameters ($P = 1$ kW, $v = 1$ m/min and $D_{def} = 30$ mm) leads to an almost pore-free microstructure, at a depth of 700 μm, possessing also reduced crack tendency and sharp normal/superconducting transition at 90 K, after oxygen annealing.

(2) In the case of HTS coatings, the application of the optimum laser treatment parameters ($P = 1$ kW, $v = 0.5$ m/min and $D_{def} = 17$ mm) lead to the fabrication of a continuous, dense and crack-free superconducting path. Non-equilibrium processing conditions lead to various characteristic solidification morphologies, in the surface of the ceramic coating, such as dendrites and radiating-aggregates (fringe-like crystals) in the LAZ. In the interior of the LAZ the presence of a complex mosaic microstructure, composed mainly of 123 grains and secondary-phase inclusions is also observed. The adhesion of the coating to the substrate was improved due to the silver diffusion at the vicinity of the interface. Post-processing heat treatment in oxygen atmosphere improves the superconducting properties of the ceramic coating, leading to a relatively wide transition at an onset critical temperature up to 90 K.

(3) Application of the thick-HTS coated silver components is evident in the construction of electrical/electronic circuits. The type of the application (electrical switches, SIS/SNS junctions) as well as the HTS components performance must be investigated further.

References

[1] M.K. Wu, J.R. Ashburn, C.J. Torng, P.H. Hor, R.L. Meng, L. Gao, Z.J. Huang, Y.O. Wang and C.W. Chu, Phys. Rev. Lett. 58 (1987) 908.
[2] S. Jin, T.H. Tiefel, R.C. Sherwood, G.W. Kammlott and S.M. Zahurak, Appl. Phys. Lett. 51 (1987) 943.
[3] K. Takahashi, S. Shimomura, A. Nagasawa, M. Ohta and K. Kakegawa, Jpn. J. Appl. Phys. Lett. 26 (1987) 1991.
[4] M. Ishii, T. Maeda, M. Matsuda, M. Takata and T. Yamashita, Jpn. J. Appl. Phys. Lett. 26 (1987) 1959.
[5] M. Kawai, T. Kawai, H. Masuhira and M. Takahashi, Jpn. J. Appl. Phys. Lett. 26 (1987) 1740.

[6] H. Koinuma, T. Hashimoto, T. Nakamura, K. Kishio, K. Kitazawa and K. Fueki, Jpn. J. Appl. Phys. Lett. 26 (1987) 761.
[7] I. Sankawa, T. Konaka, T. Matsuura and K. Ishihara, Jpn. J. Appl. Phys. Lett. 27 (1988) 1083.
[8] D.D. Berteley, D.H. Kim, B.R. Johnson, A.M. Goldman, M.L. McCartney, K. Beauchamp and J. Maps, Appl. Phys. Lett. 53 (1988) 708.
[9] K. Maeda, N. Sakamoto, Y. Namiki, Y. Aoki, T. Shiono, H. Yamamoto and M. Tanaka, in: Proc. First ISS (1988, Nagoya, Japan) p. 533.
[10] K. Shinohara, F. Munakata and M. Yamanaka, in: Proc. First ISS (1988, Nagoya, Japan) p. 489.
[11] T. Venkatesan, X.D. Wu, A. Inam, Y. Jeon, M. Croff, E.W. Chase, C.C. Chang, J.B. Wachtman, R.W. Odom, F.R. di-Brozelo and I.A. Magee, Appl. Phys. Lett. 53 (1988) 1431.
[12] O. Auciello, Mater. Manuf. Proc. 6 (1991) 33.
[13] M. Gerri, W. Marine, M. Sentis and P. Delaporte, in: Proc. 4th Int. Conf. Surface Modification Technologies (SMT4) (1991, Paris, France) p. 181.
[14] M.M. Bedekar, A. Safari and W. Wilber, Physica C 202 (1992) 42.
[15] S.K. Singh, T.J. Jackson and S.B. Palmer, Supercond. Sci. Tech. 8 (1995) 403.
[16] J. Chrzanowski, S. Meng-Busani, A.E. Curzon, J.C. Irwin, B. Heinrich, R.A. Gragg, C. Backhouse, V. Angus, F. Habilo, H. Zhouand and A.A. Fife, Supercond. Sci. Tech. 8 (1995) 455.
[17] A.G. Mamalis, A. Szalay, D.I. Pantelis, G. Pantazopoulos, I. Kotsis and M. Enisz, Supercond. Sci. Tech. 8 (1995) 471.
[18] A. Cheene, G. Maze, M. Manot, F. Queyroux, G. Dufour, H. Roulet, G. Hauchecorne, F. Kerherve, R.M. Defourneau and J. Pewiere, in: Proc. ICMAS 89 (1989, Paris, France) p. 265.
[19] C.W. Chen, P.A.A. Khan and K. Mukherjee, J. Mater. Sci. 27 (1992) 3221.
[20] V. Djafari, D. Pantelis, D. Francois and A. Rist, Memoires et Etudes Scientifiques Revue de Metallurgie. 9 (1989) 487.
[21] D. Pantelis and V. Djafari, French Patent (1989).
[22] M. Okutomi, H. Nomura and A. Kitagawa, Mater. Manuf. Proc. 6 (1991) 257.
[23] D.I. Pantelis, A.G. Mamalis and G. Pantazopoulos, in: Proc. 4th EUROMAT (1995, Padua, Italy) p. 349.
[24] D. Pantelis, Techniques de l' Ingenieur: Traite Metallurgie (1993) M1240.
[25] R.E. Muenchausen, M. Hawley, S.R. Foltyn, X.D. Wu, R.C. Dye, F.H. Garzon, G.L. Skofronick and A.H. Carim, Physica C 199 (1992) 445.